Electrochemical Detection of Human Cytochrome P450 2A6 Inhibition: A Step toward Reducing Dependence on Smoking

ARTICLE *in* ANALYTICAL CHEMISTRY · FEBRUARY 2014

Impact Factor: 5.64 · DOI: 10.1021/ac4041839 · Source: PubMed

6 AUTHORS, INCLUDING:

Silvia Castrignanò
Università degli Studi di Torino
15 PUBLICATIONS **59** CITATIONS
SEE PROFILE

Sheila J Sadeghi
60 PUBLICATIONS **827** CITATIONS
SEE PROFILE

Paola Allegra
Università degli Studi di Torino
22 PUBLICATIONS **363** CITATIONS
SEE PROFILE

Gianfranco Gilardi
Università degli Studi di Torino
124 PUBLICATIONS **2,227** CITATIONS
SEE PROFILE

analytical chemistry

Article

pubs.acs.org/ac

Electrochemical Detection of Human Cytochrome P450 2A6 Inhibition: A Step toward Reducing Dependence on Smoking

Silvia Castrignanò,[†] Alex Ortolani,[†] Sheila J. Sadeghi,[†,‡] Giovanna Di Nardo,[†] Paola Allegra,[†] and Gianfranco Gilardi*[,†,‡]

[†]Department of Life Sciences and Systems Biology, University of Torino, 10123 Torino, Italy

[‡]Centre for Nanostructured Interfaces and Surfaces, University of Torino, via Pietro Giuria 7, 10125 Torino, Italy

ABSTRACT: Inhibition of human cytochrome P450 2A6 has been demonstrated to play an important role in nicotine metabolism and consequent smoking habits. Here, the "molecular Lego" approach was used to achieve the first reported electrochemical signal of human CYP2A6 and to improve its catalytic efficiency on electrode surfaces. The enzyme was fused at the genetic level to flavodoxin from *Desulfovibrio vulgaris* (FLD) to create the chimeric CYP2A6-FLD. Electrochemical characterization by cyclic voltammetry shows clearly defined redox transitions of the haem domain in both CYP2A6 and CYP2A6-FLD. Electrocatalysis experiments using coumarin as substrate followed by fluorimetric quantification of the product were performed with immobilized CYP2A6 and CYP2A6-FLD. Comparison of the kinetic parameters showed that coumarin catalysis was carried out with a higher efficiency by the immobilized CYP2A6-FLD, with a calculated k_{cat} value significantly higher ($P < 0.005$) than that of CYP2A6, whereas the affinity for the substrate (K_M) remained unaltered. The chimeric system was also successfully used to demonstrate the inhibition of the electrochemical activity of the immobilized CYP2A6-FLD, toward both coumarin and nicotine substrates, by tranylcypromine, a potent and selective CYP2A6 inhibitor. This work shows that CYP2A6 turnover efficiency is improved when the protein is linked to the FLD redox module, and this strategy can be utilized for the development of new clinically relevant biotechnological approaches suitable for deciphering the metabolic implications of CYP2A6 polymorphism and for the screening of CYP2A6 substrates and inhibitors.

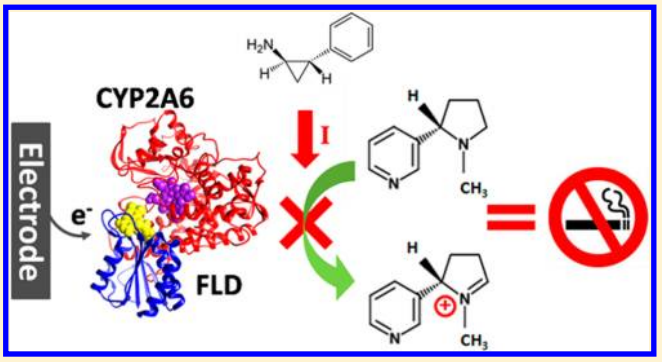

Human cytochrome P450 2A6 (CYP2A6) is a polymorphic phase I drug metabolizing enzyme representing up to 10% of total CYPs present in the liver, where it is mainly expressed.[1] There is considerable interest in CYP2A6 primarily due to its leading role in the human metabolism of nicotine, the addictive agent present in tobacco. About 80% of nicotine is metabolized by CYP2A6, and a clear relationship between CYP2A6 polymorphism and dependence from smoking has been demonstrated, together with the consequent risk of lung cancer.[2,3] It has been widely reported that the individual variability in nicotine metabolism rate, including ethnic group and gender-related differences, is highly correlated to CYP2A6 genetic polymorphism.[2] In particular, it has been observed that subjects with a genetic basis for slow CYP2A6 metabolism smoke fewer cigarettes and are more likely to stop smoking, compared to individuals with faster metabolism.[2,3] For these reasons, the use of CYP2A6 inhibitors has been suggested as a possible treatment strategy for tobacco-dependent smokers.[4]

Among drugs and xenobiotics that can be suitable for CYP2A6 inhibition, methoxsalen, a clinically approved drug for the treatment of psoriasis, has been proposed to reduce smoking behavior,[5] but it may not be selective for CYP2A6 and could increase the risk of undesirable drug−drug interactions. In addition, grapefruit juice, whose inhibitory characteristic of CYPs is well-established, has been proposed as a natural remedy, because its consumption can inhibit coumarin metabolism in vivo.[6] Other attempts have also been made to produce synthetic CYP2A6 inhibitors by mimicking the chemical structure of nicotine.[7] The discovery and improvement of new powerful and selective CYP2A6 inhibitors with low or no risk of undesirable side effects is an ongoing research area. Therefore, the development of new bioanalytical methods suitable for the screening of CYP2A6 substrates and inhibitors together with metabolic implications of CYP2A6 polymorphism is extremely desirable and of high clinical relevance, and this is the aim of the present work.

A well-known substrate of CYP2A6 is coumarin, the simplest member of plant-derivative benzopyrones.[8] In humans around 80% of coumarin is metabolized by CYP2A6, and its 7-hydroxylation is commonly used both in vitro and in vivo as a probe of CYP2A6 activity.[1,8] Coumarin derivatives are extensively used as anticoagulant and antithrombotic agents.[9,10]

Received: December 23, 2013
Accepted: February 5, 2014

   dx.doi.org/10.1021/ac4041839 | *Anal. Chem.* XXXX, XXX, XXX−XXX

Due to their biotechnological potential and relevance to drug metabolism, CYPs have received considerable attention for the development of bioelectrochemical platforms suitable for substrate and inhibitor screening.[11−20] Particular interest has been focused on the improvement of the electronic coupling of the enzyme with the electrode surface and of its catalytic efficiency. In a fully coupled system, consumption of reducing equivalents and molecular oxygen is stoichiometrically equivalent to the product formed, whereas in uncoupled systems, reducing equivalents are wasted in superoxide and hydrogen peroxide production, resulting in an impairment of the enzyme catalytic activity.[16] In order to address these difficulties, significant improvement has been made by optimizing advanced methods for electrode surface modification in conjunction with the development of appropriate protein engineering strategies.[16,17,19] To this end, our group has previously developed and implemented the so-called "molecular Lego" approach[21−25] based on the genetic fusion of electron transfer modules such as *Desulfovibrio vulgaris* flavodoxin (FLD) to the CYP of interest resulting in active multidomain P450 enzymes. In particular, it has been demonstrated that using artificial redox chains, it is possible to regulate the electron flow from the electrode to the catalytic domain by mediation of the artificial reductase domain, thus enhancing coupling efficiency and catalytic activity.[16,26]

Here, we apply the "molecular Lego" approach to improve the catalytic efficiency of CYP2A6 by fusing it at the genetic level with the FLD redox module, which is chosen for its high sequence similarity to the FMN binding domain of the class II CYP reductases.[21] Electrochemical study of CYP2A6-FLD is performed by immobilizing the fusion protein on a poly diallyldimethylammonium chloride (PDDA)-modified glassy carbon electrode, and results obtained are compared to those relative to CYP2A6 enzyme as a control. The rate of electron flow through the CYP2A6-FLD redox chain is also estimated by applying Laviron's theory[27] using cyclic voltammetry. Furthermore, the catalytic performance of CYP2A6-FLD is investigated using the well-known substrate coumarin. We examine CYP2A6-FLD turnover efficiency in the presence of coumarin by chronoamperometric electrocatalysis on the glassy carbon immobilized enzyme in comparison to CYP2A6. In addition, coupling efficiency of the enzyme is examined during coumarin electrocatalysis by online measurement of hydrogen peroxide formed using a screen-printed platinum electrode. Finally, the inhibition of immobilized CYP2A6-FLD in the presence of tranylcypromine, a potent and selective CYP2A6 inhibitor, is demonstrated toward coumarin and nicotine electrocatalysis.

EXPERIMENTAL SECTION

Chemicals. Analytical grade chemicals were used with no further purification. All solutions were prepared with ultrapure deionized water. Coumarin, 7-hydroxy-coumarin, nicotine, tranylcypromine (Sigma-Aldrich), and nicotine-Δ1′(5′)-iminiumdiperchlorate salt (Biozol) solutions were prepared just before use by dissolving the adequate amount in the appropriate solvent. Poly diallyldimethylammonium chloride (PDDA) (Sigma-Aldrich) was used without dilution.

Engineering, Expression, and Purification of CYP2A6 and CYP2A6-FLD. The Cyp2A6 gene was modified at the 5′-end, corresponding to the N-terminus of the protein, in order to remove the hydrophobic membrane anchor by deleting the first 22 amino acids using the primer 2A6 FW reported below. This was done with the aim of improving the expression and stability of the construct, as previously reported.[28] The cyp2A6 gene was amplified by PCR using the forward and reverse primers (restriction enzyme sites shown in bold) and subsequently ligated into the pCW expression vector. Primers were 5′ CAA GAT ACT ACC CAT ATG GCG AAA AAG ACC TCG AGC AAG GGG AAG CTG 3′ (2A6 forward) and 5′ TTC CTG CCC CGC CAC CAT CAC CAT TGA AAG CTT GCG AGG GCT 3′ (2A6 reverse).

Cyp2A6-FLD was cloned into pCW expression vector starting from CYP2A6 clone. Two primers, reported below, were used to amplify and modify the existing Cyp2A6 in order to delete the stop codon and to insert a unique AvrII restriction site. The AvrII restriction site allowed for the cloning of the modified Cyp2A6 gene into the pCW expression vector already containing the sequence coding for the FLD gene.[23,24]. Primers were 5′ CAA GAT ACT ACC CAT ATG GCG AAA AAG ACC TCG AGC AAG GGG AAG CTG 3′ (2A6 forward) and 5′ CCA CGA AAC TAC ACC ATG AGC TTC CTG CCC CGC CCT AGG AAT TAA 3′ (2A6 reverse).

Both clones were sequenced in order to confirm the correct amino acid sequence. As previously reported,[23,24] CYP2A6 and CYP2A6-FLD fusion proteins were expressed in *E. coli* DH5α cells with a six histidine tag at the C-terminus. The resulting recombinant proteins were purified by coupling ionic exchange (DEAE fast flow) and Ni-affinity chromatography. Both CYP2A6 and CYP2A6-FLD were stored in 50 mM phosphate buffer pH 7.4 with 20% glycerol at −20 °C.

Fourier Transform Infrared Spectroscopy (FTIR). Infrared spectra of CYP2A6 were acquired using the attenuated total reflectance (ATR) tool (Harrick Scientific Products, U.S.A.). Protein samples were prepared on gold-PET flat surface substrates following the same procedure described for glassy carbon electrodes and compared with samples prepared by gently mixing equal volumes of enzyme solution and buffer (50 mM phosphate buffer pH 7.4 with 20% glycerol). Before the FTIR analysis, samples were kept overnight at 4 °C. All spectra were collected from 4000 to 800 cm^{-1} using a Bruker Model Tensor 27 FT-IR spectrometer (Bruker Instruments, U.S.A.) with a scan velocity of 10 kHz and a resolution of 4 cm^{-1}.[29] During data acquisition, the spectrometer was continuously purged with nitrogen at room temperature. Data were collected in triplicate, and spectra were averaged using the Opus software (Bruker Instruments, U.S.A.). Spectra of the protein were collected in triplicate, subsequently averaged, and then corrected by subtraction of control samples acquired under the same scanning and temperature conditions. In particular, IR spectra of buffer or PDDA were used with the same dilution as background for enzyme samples.

Immobilization on Glassy Carbon Electrodes. Both CYP2A6 and CYP2A6-FLD proteins were immobilized on PDDA-modified glassy carbon electrodes (diameter of 0.07 cm^2, BASi, U.K.). To this end, a 1:1 mixture of PDDA/protein was cast onto clean glassy carbon electrodes and allowed to set overnight at 4 °C.

Cyclic Voltammetry and Chronoamperometry. All electrochemical experiments were carried out at room temperature (25 °C) and in 50 mM phosphate buffer pH 7.4, containing 100 mM KCl as supporting electrolyte, using an Autolab PGSTAT12 potentiostat (Ecochemie, The Netherlands) controlled by GPES3 software. A conventional three-electrode glass cell, equipped with a platinum wire counter electrode, an Ag/AgCl (3 M NaCl) reference electrode, and a 3

dx.doi.org/10.1021/ac4041839 | Anal. Chem. XXXX, XXX, XXX−XXX

mm diameter glassy carbon working electrode (BASi, U.K.), was also used.

Electrochemical investigation of CYP2A6 and CYP2A6-FLD properties was performed by cyclic voltammetry, and the potential was scanned between 400 and −850 mV at a scan rate of 120 mV/s. Cyclic voltammetry experiments were performed in a nitrogen atmosphere within a glovebox (Belle Technologies, U.K.).

Electrochemically driven substrate catalysis by CYP2A6 and CYP2A6-FLD was performed using chronoamperometry with an applied potential bias of −650 mV for 30 min. In order to ensure the substrate permeation into the enzymatic layer and minimize mass transport influence at the transducer surface, both CYP2A6 and CYP2A6-FLD were immobilized through PDDA on glassy carbon rotating disk electrodes. All chronoamperometric electrocatalysis experiments were performed at 200 rpm rotation speed using a BASi RDE-2 rotator system (Bioanalytical Systems, Inc., U.S.A.). The chronoamperometric procedure was applied on freshly prepared electrodes in the presence of increasing concentrations of substrate, and the product obtained after the 30 min reaction was immediately quantified by fluorescence spectroscopy detection in the case of coumarin and by high performance liquid chromatography (HPLC) in the case of nicotine.

The coupling efficiency of the immobilized enzymes was measured during the electrocatalysis of coumarin (saturating concentration = 10 μM) using the above-mentioned procedure. In particular, the amount of hydrogen peroxide produced was estimated using miniaturized screen-printed platinum electrodes (BVT Technologies, Czech Republic) by sampling 30 μL of the electrocatalysis solution every 5 min. Hydrogen peroxide quantification was performed on a platinum screen-printed electrode, after calibration with standard solutions, in chronoamperometry by applying a potential of 600 mV for 5 min and by measuring the steady-state current. Hydrogen peroxide concentration was estimated using the calibration curve after volume-appropriate correction. As a control experiment, ethanol (used for dissolving coumarin), instead of the substrate, was added to both CYP2A6 and CYP2A6-FLD electrodes.

Inhibition studies were carried out on CYP2A6-FLD glassy carbon electrodes using chronoamperometry, with the same parameters mentioned above for coumarin and nicotine electrocatalysis. Inhibition experiments were performed in the presence of coumarin (10 μM) or nicotine (150 μM) as the substrate and increasing concentrations of tranylcypromine (from 0.01 to 100 μM) as the inhibitor. The decrease in the amount of 7-hydroxy coumarin formed in the presence of the tranylcypromine inhibitor during coumarin electrocatalysis was calculated by fluorescence spectroscopy. The decrease in the amount of nicotine-Δ1′(5′)-iminium ion formed in the presence of the tranylcypromine inhibitor during nicotine electrocatalysis was estimated by HPLC.

Fluorescence Spectroscopy. Following the termination of the chronoamperometric experiments in the presence of different concentrations of the substrate coumarin, the electrochemical cell contents were transferred to a fluorimeter for the subsequent 7-hydroxy coumarin product quantification. Fluorescence spectra were recorded at room temperature with a Perkin-Elmer LS 55 fluorescence spectrometer (Perkin-Elmer, U.S.A.). The excitation wavelength was set at 325 nm, and emission was monitored between 400 and 600 nm with a detected maximum emission at 450 nm. Excitation and emission slit sizes were set at 4 and 6 nm, respectively.

HPLC. The quantification of nicotine electrocatalysis product formation was achieved by HPLC coupled with a diode array UV detector (Agilent-1200, Agilent technologies, U.S.A.) equipped with a 4.6 × 150 mm, 5 μm Eclipse XDB-C18 column. For this purpose, standard solutions of nicotine and Δ1′(5′)-iminium ion were separated using a linear gradient elution programmed as follows: linear gradient elution from 20% to 50% acetonitrile and 80% to 50% 20 mM phosphate buffer pH 7, 0−10 min; isocratic elution of 50% acetonitrile and 50% 20 mM phosphate buffer pH 7, 10−24 min; linear gradient elution to 20% acetonitrile and 80% 20 mM phosphate buffer pH 7, 24 min or end of the run. Flow rate was set to 1 mL/min. Detection wavelength was set to 257 nm. Retention times were 3 and 21 min for Δ1′(5′)-iminium ion and nicotine, respectively.

RESULTS AND DISCUSSION

CYP2A6 and CYP2A6-FLD were expressed in *E. coli* and purified using the protocols established in our lab for other CYPs and reported previously.[23] Reduction of the haem followed by bubbling of carbon monoxide in both purified proteins showed a complete spectral shift of the Soret peak at 418 nm to the expected 450 nm, indicating the presence of an active enzyme.

Prior to the electrochemical experiments, ATR-FTIR analysis was carried out to assess the structural integrity of the catalytic domain in the presence and absence of the cationic polyelectrolyte PDDA (poly diallyldimethylammonium chloride). In particular, the spectral region included between 1450 and 1750 cm^{-1} was considered, which contains information on protein secondary structure composition. As shown in Figure 1,

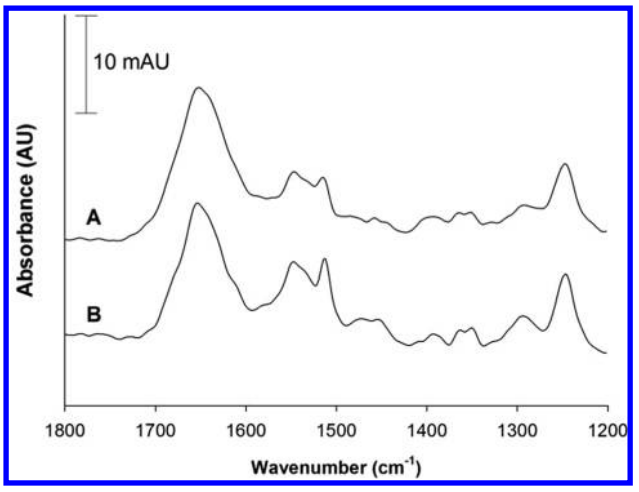

Figure 1. FTIR spectra of (A) CYP2A6 and (B) CYP2A6 in the presence of PDDA. Spectra were collected in triplicate and subsequently averaged and corrected by background subtraction.

spectra obtained for both CYP2A6 in the absence and in the presence of PDDA are essentially similar and exhibit the amide I and II bands, which are characteristics of the secondary structure of proteins.[30] The amide I band (~1650 cm^{-1}) consists of a group of overlapped signals, mainly due to the peptidic carbonyl group stretching mode with a minor contribution from the out-of-phase C−N stretching vibration.[30] Grouped bands centered at around 1550 cm^{-1} are commonly

dx.doi.org/10.1021/ac4041839 | Anal. Chem. XXXX, XXX, XXX−XXX

assigned to the amide II band, which corresponds to the out-of-phase combination of the peptidic N−H in-plane bend and the C−N stretching vibration. Additionally, the peak at 1517 cm^{-1} can be assigned to the C−C stretch and C−H bend of side chain tyrosine residues.[30] Moreover, a set of bands that can be assigned to the amide III are also clearly detectable in the region between 1200 and 1400 cm^{-1}. The latter signals are related to the in-phase combination of the peptidic N−H and C−N bonds bending vibration.[30]

The ATR-FTIR data show that the catalytic domain is not denatured upon immobilization and that the secondary structure of CYP2A6 is not affected by the presence of PDDA. Subsequently, direct electrochemistry of both enzymes was performed using cyclic voltammetry on PDDA-modified glassy carbon electrodes. Cyclic voltammograms of CYP2A6 and CYP2A6-FLD collected under anaerobic conditions are reported in Figure 2, where a redox couple corresponding to haem $Fe^{III/II}$ transition with a midpoint potential of about −230 mV is shown.

An additional redox couple is observed in the cyclic voltammogram of CYP2A6-FLD and is assigned to the semiquinone−hydroquinone transition of the FMN cofactor with a midpoint potential of about −660 mV. No voltammetric peaks are observed in the absence of enzyme (data not shown). Peak-to-peak separation of about 130 mV for the haem $Fe^{III/II}$ transition and 180 mV for the FLD semiquinone−hydroquinone indicate a quasi-reversible electrochemical processes typical of slow electron transfer kinetics. The electron transfer rate constant (k_s) was also calculated from empirically fitted Laviron's equations.[27] In particular, irreversible electrochemistry of both CYP2A6 and CYP2A6-FLD PDDA-immobilized proteins was studied by cyclic voltammetry with an increase in the scan rate from 0.2 to 0.5 V s^{-1}, and the cathodic and anodic peak potentials were plotted versus the logarithm of the scan rate. The k_s values were calculated from the intercept of the plot of E versus ln ν and were determined to be 0.13 s^{-1} for CYP2A6 and 0.08 s^{-1} for CYP2A6-FLD. As previously reported,[19] low electron transfer rate is essential for electrochemically driven catalysis of P450 systems, because it allows for the fine-tuning of the electron delivery from the reductase to the haem catalytic site. A summary of electrochemical data calculated for CYP2A6 and CYP2A6-FLD is reported in Table 1.

The activity of both CYP2A6 and CYP2A6-FLD using coumarin as the marker substrate was investigated by chronoamperometric delivery of reducing equivalents to the immobilized enzymes in the presence of increasing concentrations of this substrate. Fluorescence detection was then used to quantify the 7-hydroxy coumarin product[31] with an excitation wavelength of 325 nm and an emission wavelength of 463 nm, as described in the Experimental Section. The results obtained using CYP2A6 and CYP2A6-FLD glassy carbon electrodes in the presence of increasing concentrations of coumarin are shown in Figure 3A,B, respectively. Michaelis−Menten curves for the turnover of both CYP2A6 and CYP2A6-FLD in the presence of coumarin were obtained by plotting the rate of product formation versus the relative coumarin concentrations (Figure 3C). As can be seen from the figure, a significant difference between CYP2A6 and CYP2A6-FLD was observed in the presence of coumarin, which was confirmed by a one-way ANOVA followed by a post hoc Tukey test (P < 0.001). K_M and k_{cat} values for the electrocatalysis of coumarin were calculated to be 1.03 ± 0.05 μM and 0.17 ± 0.01 min^{-1}

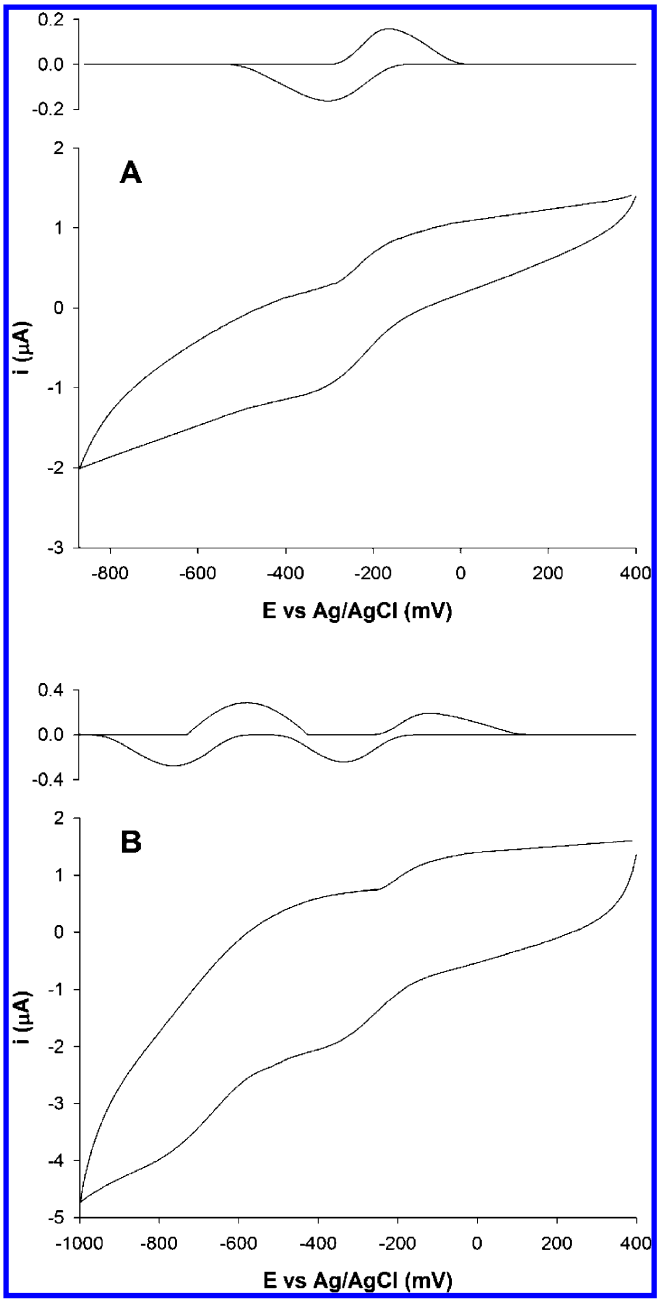

Figure 2. Anaerobic cyclic voltammograms of CYP2A6 (A) and CYP2A6-FLD (B) on PDDA-modified glassy carbon electrodes. Shown are the original and baseline corrected (upper traces) cyclic voltammograms. Scan rate: 120 mV s^{-1} in in 50 mM potassium phosphate buffer pH 7.4 with 100 mM KCl at 25 °C.

for CYP2A6 and 1.00 ± 0.28 μM and 0.28 ± 0.01 min^{-1} for CYP2A6-FLD. Results from a student's t test showed no differences when evaluating K_M values, whereas a significant difference between CYP2A6 and CYP2A6-FLD was found when comparing k_{cat} values. In particular, the k_{cat} value of coumarin electrocatalysis was significantly higher for CYP2A6-FLD than for CYP2A6 (P < 0.005).

Kinetic values obtained for CYP2A6 have been compared in Table 2 with previously published results for coumarin catalysis.[32−35] Because to our knowledge this is the first report of the immobilization of CYP2A6, the values reported in the latter table are those of the recombinant enzyme free in solution and not immobilized. Regarding the K_M values, our

dx.doi.org/10.1021/ac4041839 | Anal. Chem. XXXX, XXX, XXX−XXX

Table 1. Redox Properties of CYP2A6 and CYP2A6-FLD Immobilized on Glassy Carbon Electrodes Modified with PDDA

	E_c (mV)	E_a (mV)	E_m (mV)	ΔE (mV)	k_s (s^{-1})
CYP2A6	−294 ± 8	−174 ± 2	−234 ± 5	121 ± 7	0.13
CYP2A6-FLD	−321 ± 12	−128 ± 4	−225 ± 4	134 ± 15	0.08
	−753 ± 7	−572 ± 6	−662 ± 6	181 ± 10	

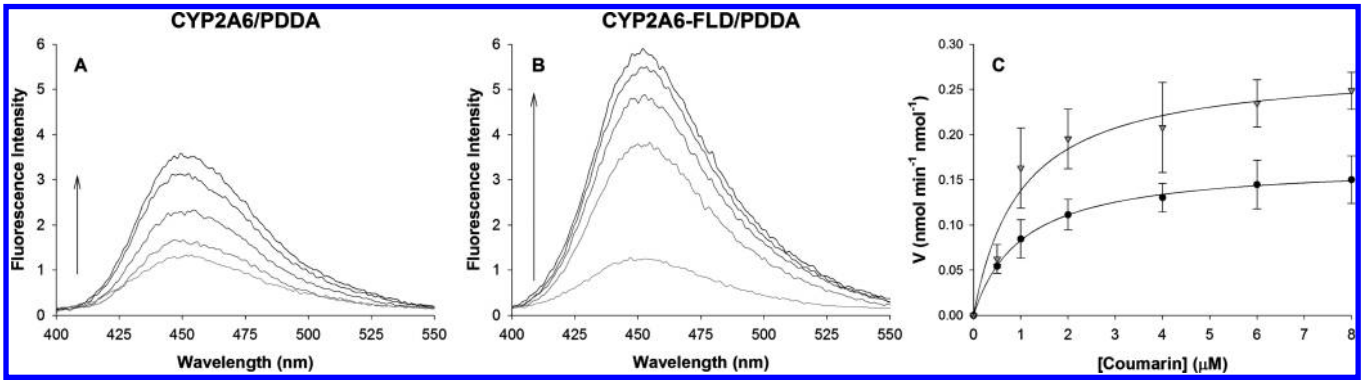

Figure 3. Formation of 7-hydroxycoumarin by CYP2A6 (A) and CYP2A6-FLD (B) immobilized on PDDA glassy carbon electrodes detected by fluorescence spectroscopy. (C) Plot of reaction velocity versus substrate concentration fitted to a Michaelis−Menten equation for CYP2A6 (circles) and CYP2A6-FLD (triangles). Data are shown as mean ± SD of three different electrodes.

Table 2. Comparison of Calculated Kinetic Parameters for Coumarin Catalysis by Immobilized CYP2A6 and Literature Data Determined on Recombinant Enzyme (Rec) Free in Solution

	K_M (μM)	k_{cat} (min^{-1})	variant, host
present work:			
2A6	1.03 ± 0.05	0.17 ± 0.01	rec, *E. coli*
2A6-FLD	1.00 ± 0.28	0.28 ± 0.01	rec, *E. coli*
Soucek, 1999[32]	1.48 ± 0.37	3.36 ± 0.18	rec, *E. coli*
He et al., 2004[33]	2.17 ± 0.63	3.23	rec, *Spodoptera frugiperda*
Fukami et al., 2005[34]	1.00 ± 0.10	5.2 ± 0.3	rec, *E. coli*
Yun et al., 2005[35]	1.80 ± 0.70	4.5 ± 0.5	rec, *E. coli*

results were found to be in the same range as those in the literature (1−2 μM), confirming the preservation of protein affinity for the substrate. However, the electrochemical k_{cat} values for both proteins were found to be lower than the values reported for CYP2A6 free in solution. It must be noted that in general the nonoriented immobilization of enzymes on electrodes does affect the turnover number, because not all the enzymes are within distances that allow for electron transfer, and this is not unique to the system described here. More interesting though is the comparison between the two immobilized proteins where the chimeric enzyme shows a higher catalytic efficiency (k_{cat}/K_M) to that of the CYP2A6 (i.e., 0.28 versus 0.17 min^{-1} μM^{-1}).

An evaluation of the coupling efficiency of immobilized CYP2A6 and CYP2A6-FLD was also carried out by measuring the hydrogen peroxide production during coumarin electrocatalysis. The chronoamperograms of sampled solutions during electrocatalysis of CYP2A6 and CYP2A6-FLD obtained using screen-printed platinum electrodes are shown in Figure 4A,B. Hydrogen peroxide production profiles (Figure 4C) were obtained by plotting the calculated hydrogen peroxide concentration values versus time for both coumarin electrocatalysis and control experiments (in the presence of only ethanol−coumarin solvent). The different hydrogen peroxide production profiles were compared by two-way ANOVA followed by a post hoc Tukey test, which showed that hydrogen peroxide produced during coumarin electrocatalysis was significantly higher for immobilized CYP2A6 than

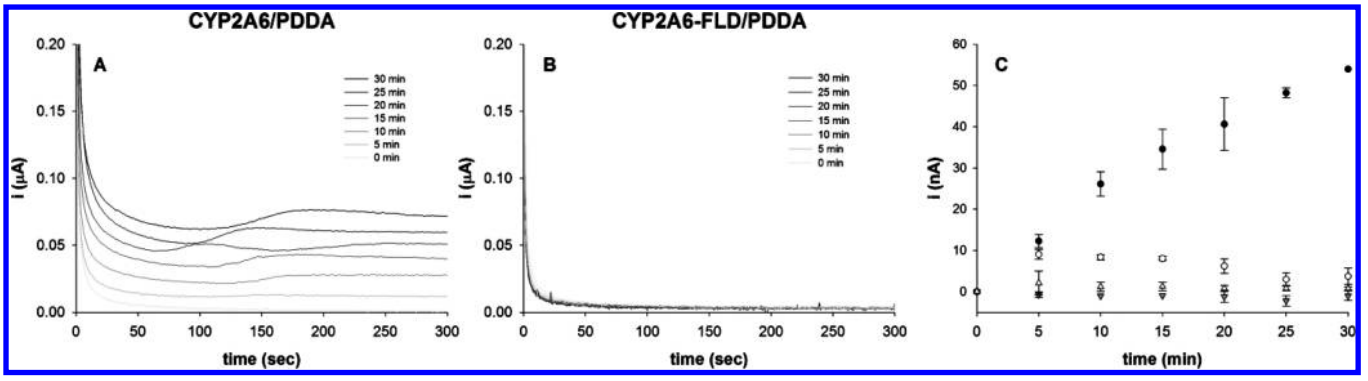

Figure 4. Estimation of the amount of hydrogen peroxide produced during coumarin electrocatalysis by CYP2A6 (A) and CYP2A6-FLD (B) performed on screen-printed platinum electrode. (C) Hydrogen peroxide production profile during coumarin electrocatalysis (filled symbols) and control experiments (empty symbols) on immobilized CYP2A6 (circles) and CYP2A6-FLD (triangles) on glassy carbon electrodes.

dx.doi.org/10.1021/ac4041839 | *Anal. Chem.* XXXX, XXX, XXX−XXX

CYP2A6-FLD ($P < 0.001$). Furthermore, on CYP2A6 glassy carbon electrodes, hydrogen peroxide was produced in statistically higher amounts during coumarin electrocatalysis than during control experiments in the presence of only buffer ($P < 0.001$). However, no significant differences were found when comparing hydrogen peroxide production during coumarin electrocatalysis, and control experiments on CYP2A6-FLD glassy carbon electrodes confirmed that the chimeric protein is more coupled. The latter observation is also supported by the fact that the immobilized CYP2A6-FLD yields double the amount of 7-hydroxycoumarin product when compared to CYP2A6 alone, as mentioned earlier (Table 2).

The data obtained demonstrate that the regulation of electron flow to the haem of immobilized CYP2A6 when genetically fused to *D. vulgaris* FLD significantly enhanced both coupling and catalytic efficiencies of this enzyme toward coumarin hydroxylation.

Finally, the improved catalytic efficiency of CYP2A6 when genetically fused to FLD was examined toward enzyme inhibition in the presence of tranylcypromine, a potent and relatively selective inhibitor of CYP2A6.[1] Tranylcypromine is a nonhydrazine monoamine oxidase inhibitor used in psychiatry[40] and has proven inhibitory activity toward many CYPs.[1] Previously published studies on human liver microsomes or cDNA-expressing microsomes have reported the inhibition of CYP2A6 activity toward coumarin 7-hydroxylation by tranylcypromine, with calculated K_i values ranging from 0.04 to 0.42 μM.[1,36,37] Here, we used CYP2A6-FLD glassy carbon electrodes to investigate the inhibition of coumarin metabolism by tranylcypromine.

The inhibition profile of CYP2A6-FLD coumarin 7-hydroxylation by tranylcypromine is shown in Figure 5. The

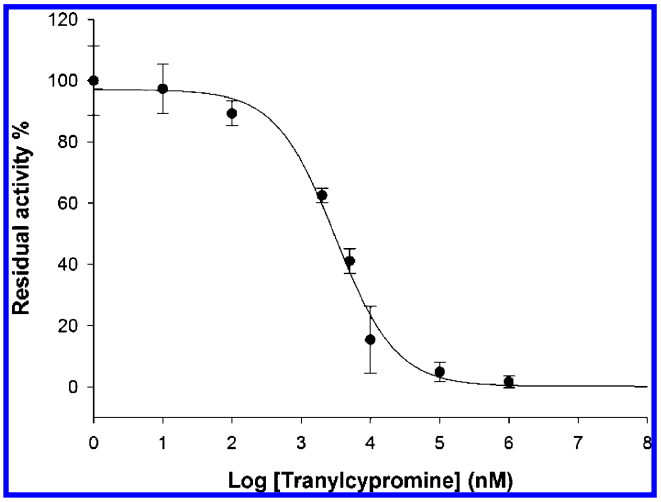

Figure 5. Tranylcypromine concentration-dependent inhibition of coumarin 7-hydroxylation by CYP2A6-FLD-modified glassy carbon electrodes. Data are shown as mean ± SD of three different electrodes.

calculated IC_{50} value was 3.1 ± 0.6 μM. Using the Cheng and Prusoff relationship for competitive inhibition, the calculated IC_{50} value was also converted to K_i, obtaining a value of 0.29 ± 0.06 μM which is in good agreement with previously published results using microsomes.[1,36,37]

In addition, inhibition experiments in the presence of tranylcypromine were also performed using nicotine as substrate. In humans, about 70 to 80% of nicotine is converted to cotinine in two enzymatic steps. The first is nicotine 5′-oxidation mediated by CYP2A6. Second, the Δ1′(5′)-iminium ion product of this reaction is further metabolized to cotinine by aldehyde oxidase.[6,39,40] Here, we first calculated the K_M value by performing electrocatalysis of nicotine on CYP2A6-FLD glassy carbon electrodes. The estimated K_M value was 131.4 ± 52.2 μM, which is in agreement with previously published results on microsomal CYP2A6 protein.[40] Subsequently, we used CYP2A6-FLD glassy carbon electrodes to investigate the inhibition of nicotine metabolism by tranylcypromine. The inhibition profile of CYP2A6-FLD nicotine 5′-oxidation by tranylcypromine is shown in Figure 6.

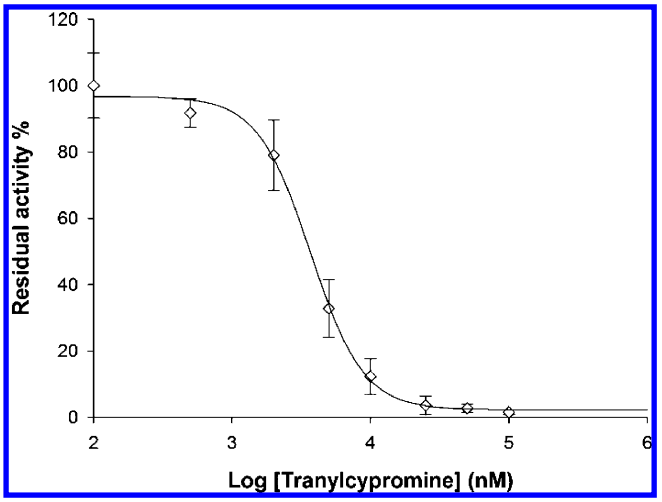

Figure 6. Tranylcypromine concentration-dependent inhibition of nicotine 5′-oxidation by CYP2A6-FLD-modified glassy carbon electrodes. Data are shown as mean ± SD of three different electrodes.

The calculated IC_{50} value was 3.7 ± 0.2 μM. Using the Cheng and Prusoff relationship for competitive inhibition,[38] the calculated IC_{50} value was also converted to K_i, obtaining a value of 1.72 ± 0.09 μM. No data regarding tranylcypromine inhibition of CYP2A6 5′-oxidation of nicotine are found in the literature to compare with our results.

CONCLUSIONS

In conclusion, for the first time, a bioelectrochemical setup suitable for the investigation of CYP2A6 catalytic activity has been developed by immobilizing on glassy carbon electrodes the chimeric form of the enzyme CYP2A6-FLD obtained by genetically fusing CYP2A6 with FLD. The fusion protein showed an improved catalytic efficiency in agreement with previously reported data on CYP3A4,[16] where the regulation of the electron flow to the haem through FLD resulted in higher amounts of product due to an enhancement of the coupling efficiency. It was also demonstrated that the increase in catalytic activity observed for CYP2A6-FLD when compared to CYP2A6 could be related to the improved control of the enzyme coupling efficiency and to a more refined electron flow tuning. The CYP2A6-based bioelectrochemical platform was also successfully used to test enzymatic inhibition in the presence of its well-known inhibiting drug, proving the suitability of this system for the screening of inhibitors of this enzyme, which is highly relevant to nicotine addiction treatment. Finally, this molecular engineering approach can aid in the development of improved electrochemical sensors

dx.doi.org/10.1021/ac4041839 | *Anal. Chem.* XXXX, XXX, XXX−XXX

based on CYP enzymes for drug screening and metabolic profiling.

AUTHOR INFORMATION

Corresponding Author

*E-mail: gianfranco.gilardi@unito.it. Fax: +39-011-6704643. Tel.: +39-011-6704593.

Author Contributions

The manuscript was written through contributions of all authors. All authors have given approval to the final version of the manuscript.

Notes

The authors declare no competing financial interest.

ACKNOWLEDGMENTS

This work was supported by the Region Piedmont CIPE 2006 (CYP-TECH project, Italy) and Progetto Ateneo-San Paolo 2012 (Torino, Italy awarded to S.J.S.).

REFERENCES

(1) Di, Y. M.; Chow, V. D.; Yang, L. P.; Zhou, S. F. *Curr. Drug Metab.* **2009**, *10*, 754−780.
(2) Malaiyandi, V.; Sellers, E. M.; Tyndale, R. F. *Clin. Pharmacol. Ther.* **2005**, *77*, 145−158.
(3) Benowitz, N. L. *Annu. Rev. Pharmacol. Toxicol.* **2009**, *49*, 57−71.
(4) Sellers, E. M.; Tyndale, R. F.; Fernandes, L. C. *Drug Discovery Today* **2003**, *8*, 487−493.
(5) Hukkanen, J.; Jacob, P., III; Benowitz, N. L. *Clin. Pharmacol. Ther.* **2006**, *80*, 522−530.
(6) Yano, J. K.; Denton, T. T.; Cerny, M. A.; Zhang, X.; Johnson, E. F.; Cashman, J. R. *J. Med. Chem.* **2006**, *49*, 6987−7001.
(7) Kontogiorgis, C.; Detsi, A.; Hadjipavlou-Litina, D. *Expert Opin. Ther. Pat.* **2012**, *22*, 437−454.
(8) Mueller, R. L. *Best Pract. Res. Clin. Haematol.* **2004**, *17*, 23−53.
(9) Fareed, J.; Thethi, I.; Hoppensteadt, D. *Annu. Rev. Pharmacol. Toxicol.* **2012**, *52*, 79−99.
(10) Fylaktakidou, K. C.; Hadjipavlou-Litina, D. J.; Litinas, K. E.; Nicolaides, D. N. *Curr. Pharm. Des.* **2004**, *10*, 3813−3833.
(11) Yarman, A.; Wollenberger, U.; Scheller, F. W. *Electrochim. Acta* **2013**, *110*, 63−72.
(12) Fantuzzi, A.; Capria, E.; Mak, L. H.; Dodhia, V. R.; Sadeghi, S. J.; Collins, S.; Somers, G.; Huq, E.; Gilardi, G. *Anal. Chem.* **2010**, *82*, 10222−10227.
(13) Schneider, E.; Clark, D. S. *Biosens. Bioelectron.* **2013**, *39*, 1−13.
(14) Fantuzzi, A.; Fairhead, M.; Gilardi, G. *J. Am. Chem. Soc.* **2004**, *126*, 5040−5041.
(15) Fantuzzi, A.; Meharenna, Y. T.; Briscoe, P. B.; Sassone, C.; Borgia, B.; Gilardi, G. *Chem. Commun.* **2006**, *12*, 1289−1291.
(16) Dodhia, V. R.; Sassone, C.; Fantuzzi, A.; Di Nardo, G.; Sadeghi, S. J.; Gilardi, G. *Electrochem. Commun.* **2008**, *10*, 1744−1747.
(17) Ferrero, V. E. V.; Andolfi, L.; Di Nardo, G.; Sadeghi, S. J.; Fantuzzi, A.; Cannistraro, S.; Gilardi, G. *Anal. Chem.* **2008**, *80*, 8438−8446.
(18) Mak, L. H.; Sadeghi, S. J.; Fantuzzi, A.; Gilardi, G. *Anal. Chem.* **2010**, *82*, 5357−5362.
(19) Sadeghi, S. J.; Fantuzzi, A.; Gilardi, G. *Biochim. Biophys. Acta* **2011**, *1814*, 237−248.
(20) Sadeghi, S. J.; Ferrero, S.; Di Nardo, G.; Gilardi, G. *Bioelectrochem.* **2012**, *86*, 87−91.
(21) Valetti, F.; Sadeghi, S. J.; Meharenna, Y. T.; Leliveld, S. R.; Gilardi, G. *Biosens. Bioelectron.* **1998**, *13*, 675−685.
(22) Sadeghi, S. J.; Meharenna, Y. T.; Fantuzzi, A.; Valetti, F.; Gilardi, G. *Faraday Discuss.* **2000**, *116*, 135−153.
(23) Dodhia, V. R.; Fantuzzi, A.; Gilardi, G. *J. Biol. Inorg. Chem.* **2006**, *11*, 903−916.
(24) Fairhead, M.; Giannini, S.; Gillam, E. M.; Gilardi, G. *J. Biol. Inorg. Chem.* **2005**, *10*, 842−853.
(25) Sadeghi, S. J.; Gilardi, G. *Biotech. Appl. Biochem.* **2013**, *60*, 102−110.
(26) Degregorio, D.; Sadeghi, S. J.; Di Nardo, G.; Gilardi, G.; Solinas, S. P. *J. Biol. Inorg. Chem.* **2011**, *16*, 109−116.
(27) Laviron, E. *J. Electroanal. Chem.* **1979**, *101*, 19−28.
(28) Yano, J. K.; Hsu, M. H.; Griffin, K. J.; Strout, C. D.; Johnson, E. F. *Nat. Struct. Mol. Biol.* **2005**, *12*, 822−823.
(29) Castrignanò, S.; Sadeghi, S. J.; Gilardi, G. *Biochim. Biophys. Acta* **2012**, *1820*, 2072−2078.
(30) Barth, A. *Biochim. Biophys. Acta* **2007**, *1767*, 1073−1101.
(31) Kim, D.; Wu, Z. L.; Guengerich, F. P. *J. Biol. Chem.* **2005**, *280*, 40319−40327.
(32) Soucek, P. *Arch. Biochem. Biophys.* **1999**, *370*, 190−200.
(33) He, X. Y.; Shen, J.; Hu, W. Y.; Ding, X.; Lu, A. Y.; Hong, J. Y. *Arch. Biochem. Biophys.* **2004**, *427*, 143−153.
(34) Fukami, T.; Nakajima, M.; Higashi, E.; Yamanaka, H.; Sakai, H.; McLeod, H. L.; Yokoi, T. *Drug Metab. Dispos.* **2005**, *33*, 1202−1210.
(35) Yun, C.-H.; Kim, K.-H.; Calcutt, M. W.; Guengerich, F. P. *J. Biol. Chem.* **2005**, *280*, 12279−12291.
(36) Taavitsainen, P.; Juvonen, R.; Pelkonen, O. *Drug Metab. Dispos.* **2001**, *29*, 217−222.
(37) Zhang, W.; Kilicarslan, T.; Tyndale, R. F.; Sellers, E. M. *Drug Metab. Dispos.* **2001**, *29*, 897−902.
(38) Copeland, R. A. *Enzymes: A Practical Introduction to Structure, Mechanism, and Data Analysis*, 2nd ed.; John Wiley & Sons: New York, 2000.
(39) Denton, T. T.; Zhang, X.; Cashman, J. R. *Biochem. Pharmacol.* **2004**, *67*, 751−756.
(40) Murphy, S. E.; Raulinaitis, V.; Brown, K. M. *Drug Metab. Dispos.* **2005**, *33*, 1166−1173.

dx.doi.org/10.1021/ac4041839 | *Anal. Chem.* XXXX, XXX, XXX−XXX